

Potential sources of contamination to weak lensing measurements: constraints from N-body simulations

Catherine Heymans^{1*}, Martin White^{2,3}, Alan Heavens⁴, Chris Vale^{5,2} & Ludovic Van Waerbeke¹

¹ Department of Physics and Astronomy, 6224 Agricultural Road, University of British Columbia, Vancouver, BC, V6T 1Z1, Canada.

² Department of Physics and Astronomy, 601 Campbell Hall, University of California Berkeley, CA 94720, USA.

³ Lawrence Berkeley National Laboratory, 1 Cyclotron Road, Berkeley, CA 94720, USA.

⁴ SUPA†, Institute for Astronomy, University of Edinburgh, Blackford Hill, Edinburgh, EH9 3HJ, UK.

⁵ Theoretical Astrophysics, Fermi National Accelerator Laboratory, Batavia, IL 60510, USA.

13 March 2018

ABSTRACT

We investigate the expected correlation between the weak gravitational shear of distant galaxies and the orientation of foreground galaxies, through the use of numerical simulations. This shear-ellipticity correlation can mimic a cosmological weak lensing signal, and is potentially the limiting physical systematic effect for cosmology with future high-precision weak lensing surveys. We find that, if uncorrected, the shear-ellipticity correlation could contribute up to 10% of the weak lensing signal on scales up to 20 arcminutes, for lensing surveys with a median depth $z_m = 1$. The most massive foreground galaxies are expected to cause the largest correlations, a result also seen in the Sloan Digital Sky Survey. We find that the redshift dependence of the effect is proportional to the lensing efficiency of the foreground, and this offers prospects for removal to high precision, although with some model dependence. The contamination is characterised by a weakly negative B-mode, which can be used as a diagnostic of systematic errors. We also provide more accurate predictions for a second potential source of error, the intrinsic alignment of nearby galaxies. This source of contamination is less important, however, as it can be easily removed with distance information.

Key words: cosmology: observations - gravitational lensing - large-scale structure.

1 INTRODUCTION

Weak gravitational lensing by large-scale structure provides a test of cosmology that is based on the well understood physics of gravity. The lensing strength is directly related to the large-scale distribution of matter and thus enables constraints to be placed on cosmological parameters such as the matter density parameter Ω_m and the amplitude of the matter power spectrum σ_8 (Van Waerbeke et al. 2001; Hoekstra et al. 2002; Bacon et al. 2003; Jarvis et al. 2003; Brown et al. 2003; Hamana et al. 2003; Massey et al. 2005; Rhodes et al. 2004; Van Waerbeke et al. 2005; Heymans et al. 2005; Semboloni et al. 2006; Hoekstra et al. 2006). Combined with redshift information, measurements of weak lensing are also able to constrain the equation of state of the dark energy $w(z)$ as lensing can probe the effect dark energy has on both the evolution of the matter power spectrum and the redshift-distance relationship. With the next generation of deep-field and wide-field

multi-colour surveys, weak lensing has the exciting prospect of providing constraints to distinguish between a cosmological constant ($w = -1$) and quintessence models ($w(z) \geq -1$).

Lensing by large-scale structure weakly distorts images of background galaxies such that the observed galaxy ellipticity

$$e_{\text{obs}} \simeq e_s + \gamma, \quad (1)$$

where e_s is the intrinsic galaxy ellipticity, or source ellipticity, and γ is the weak lensing shear distortion. Lensing by large-scale structure is coherent and hence it induces weak correlations in the observed ellipticities of galaxies such that $\langle e_{\text{obs}}^a e_{\text{obs}}^b \rangle_\theta > 0$, where the average is taken over all galaxy pairs (a, b) separated by angle θ . From equation 1,

$$\langle e_{\text{obs}}^a e_{\text{obs}}^b \rangle = \langle e_s^a e_s^b \rangle + \langle \gamma^a e_s^b \rangle + \langle \gamma^b e_s^a \rangle + \langle \gamma^a \gamma^b \rangle. \quad (2)$$

In order to extract the weak cosmological signal $\langle \gamma^a \gamma^b \rangle$ from the observed galaxy ellipticity correlation $\langle e_{\text{obs}}^a e_{\text{obs}}^b \rangle$, all intrinsic terms including e_s are typically assumed to be negligible. There are however potential physical limitations to this assumption related to correlations between galaxy shape and the den-

* heymans@physics.ubc.ca

† Scottish Universities Physics Alliance

sity field. This could arise, for example, through tidal torques operating during galaxy formation (Hoyle 1949; Peebles 1969; Heavens & Peacock 1988). Such a correlation would introduce an intrinsic alignment between nearby galaxies mimicking the weak lensing effect, i.e. if galaxies a and b were physically close $\langle e_s^a e_s^b \rangle \neq 0$. Investigated observationally (Brown et al. (2002); Lee et al. (2002); Heymans et al. (2004), hereafter H04, Mandelbaum et al. (2006)), analytically (Catelan et al. 2001; Crittenden et al. 2001; Lee & Pen 2001; Porciani et al. 2002; Mackey et al. 2002) and through numerical simulations (Heavens et al. (2000), hereafter HRH, Croft & Metzler (2000); Jing (2002), H04), it is currently thought that this intrinsic alignment effect is weak, at the level of a few percent contamination to the lensing signal from a deep survey of median redshift $z_m \sim 1$. Division of a redshift survey for lensing tomography (see for example Hu 1999), however, significantly increases the contamination in the lower redshift bins (H04). As shown by Heymans & Heavens (2003) and King & Schneider (2002) this contamination can be effectively removed at high accuracy by optimally downweighting pairs of nearby galaxies in the lensing analysis (see H04 for an implementation of this method). Hence this physical systematic need not limit the accuracy of future multi-colour weak lensing surveys.

Correlations between a galaxy’s shape and its surrounding density field may also introduce another more subtle effect, first discussed by Hirata & Seljak (2004). Consider the image of a distant galaxy lensed by the dark matter density surrounding a foreground galaxy. If the shape of the foreground galaxy is correlated with the tidal gravitational field, this could lead to a non-zero correlation¹ between intrinsic foreground galaxy ellipticity e_s and the lensing shear distortion experienced by the distant galaxy γ , i.e. if galaxy a is always more distant than galaxy b , $\langle \gamma^a e_s^b \rangle \neq 0$. Hirata & Seljak (2004) explore two analytical models to estimate the magnitude of this effect finding that when galaxy ellipticity is quadratically related to the tidal or density field, as suggested by tidal torque theory, no shear-ellipticity correlation is found. When galaxy ellipticity is linearly related to the tidal or density field, however, the shear-ellipticity correlation can be similar to the magnitude of the weak lensing shear correlation. In this model, galaxies are assumed initially to be spherical and acquire ellipticity by responding to the linear tidal field. For a spherically symmetric overdensity, the tidal field compresses the spherical galaxy along the direction to the over-density centre. Around a spherically symmetric proto-void, the linear theory would stretch the galaxy along the direction to the void centre. There is some observational evidence to support the linear model from Trujillo et al. (2006), who find that the rotation axes of galaxies located near voids are preferentially aligned with the void surface.

If a shear-ellipticity correlation does exist then its strength is expected to be dependent on the lensing efficiency of the lens-source pair (Hirata & Seljak 2004). King (2005) has developed this idea to show that using correlation function tomography and knowledge of the redshift dependence of each source of contamination, one could separate the true cosmological lensing signal from both the intrinsic galaxy alignment contamination and the shear-ellipticity correlation contamination.

The shear-ellipticity correlation effect has recently been inves-

tigated observationally by Mandelbaum et al. (2006) who measure the correlation between the intrinsic ellipticities of nearby galaxies and the density field that surrounds them in the Sloan Digital Sky Survey (SDSS). As the density field is responsible for the gravitational lensing of background galaxies, Mandelbaum et al. (2006) are able to estimate the shear-ellipticity correlation for any lensing survey. They find that for most galaxy types, the shear-ellipticity correlation is consistent with no signal. The shapes of the most luminous red galaxies are however found to be strongly correlated with the density field. For a lensing survey with a median source redshift $z_m \sim 1$ the most luminous galaxies would then introduce a shear-ellipticity correlation signal that is found to be at a similar magnitude to the pure lensing correlation signal from a Λ CDM cosmology. Averaging over the full galaxy sample, Mandelbaum et al. (2006) suggest that there would be a $\sim 5\%$ contamination to the pure lensing signal. These results are however subject to noise (the results for the full galaxy sample are also consistent with zero contamination), and are based on measurements taken at very low redshift and projected to the higher redshifts that are probed by lensing surveys. In this paper we therefore aim to address this issue through the analysis of extensive numerical dark matter simulations (Vale & White 2003), following the philosophy of HRH and H04 whereby galaxy ellipticity is defined from the properties of the parent dark matter halos.

This paper is organised as follows. In section 2 we describe the N-body simulations that we use in this analysis and the different models used to populate dark matter halos with luminous galaxies. We update the results of HRH and H04 in section 3 by presenting higher signal-to-noise measurements of the E and B-mode intrinsic alignment correlation $\langle e_s^a e_s^b \rangle_\theta$ from our N-body simulations and we compare these results to the recent observational measurements of Mandelbaum et al. (2006). We also investigate the effect of nearby voids on galaxy shape and compare our results to the observational measurements of Trujillo et al. (2006). In section 4 we present measurements of the E and B-mode shear-ellipticity correlation $\langle \gamma^a e_s^b \rangle$ and measure the redshift dependence of this signal. This allows us to provide fitting formulae for the shear-ellipticity correlation measured from different galaxy models. We discuss our findings in section 5 and conclude in section 6.

2 N-BODY SIMULATIONS

The basis of our calculation is a large N-body simulation of a Λ CDM cosmology. The simulation used 512^3 particles in a periodic cubic box $300h^{-1}\text{Mpc}$ on a side. This represents a large enough cosmological volume to ensure a fair sample of the Universe, while maintaining enough mass resolution to identify galactic mass halos. The cosmological model is chosen to provide a reasonable fit to a wide range of observations with $\Omega_m = 0.3$, $\Omega_\Lambda = 0.7$, $H_0 = 100 h \text{ kms}^{-1}\text{Mpc}^{-1}$ with $h = 0.7$, $\Omega_B h^2 = 0.02$ and a scale-invariant spectrum with $\sigma_8 = 0.8$. The simulation was started at $z = 60$ and evolved to $z = 0$ using the TreePM code of White (2002). The full phase space distribution was recorded every $100h^{-1}\text{Mpc}$ from $z \simeq 2$ to $z = 0$. The gravitational force softening was of a spline form, with a “Plummer-equivalent” softening length of $20 h^{-1}\text{kpc}$ comoving. The particle mass is $1.7 \times 10^{10} h^{-1} M_\odot$ allowing us to find bound halos with masses several times $10^{11} h^{-1} M_\odot$.

For each output we determine the halo catalogue by running a “friends-of-friends” (FoF) group finder (e.g. Davis et al. (1985)) with a linking length $b = 0.15$ in units of the mean inter-particle

¹ We hereafter refer to this effect as a shear-ellipticity correlation. In the literature Hirata & Seljak (2004) and King (2005) refer to this effect as intrinsic alignment-lensing interference and Mandelbaum et al. (2006) use the term GI contamination.

spacing. This procedure partitions the particles into equivalence classes, by linking together all particle pairs separated by less than a distance b . This means that FoF halos are bounded by a surface of density roughly 140 times the background density. For each halo we computed the angular momentum and the moment of inertia tensor, using the centre of mass of the particles in the FoF group as the centre of the halo.

A past light cone was constructed by stacking the boxes back along the line of sight, with boxes shifted by random amounts in the x - and y -directions and viewed down randomly chosen axes to avoid artificial periodicity. The full projected mass distribution was used to create convergence maps of κ at a source redshift plane of $z_s \sim 1$ and $z_s \sim 0.5$, where κ is defined to be the dimensionless surface mass density. The gravitational shear $\gamma = (\gamma_1, \gamma_2)$ that a galaxy at $z_s \sim 1$, or $z_s \sim 0.5$ would experience is then created from the κ maps (Kaiser & Squires 1993). The halo information was transformed into the same coordinate system to create a light cone halo distribution. 12 different realizations of the 2048^2 pixel maps were made in all, each with a 25 square degree field-of-view.

2.1 Galaxy Models

From a catalogue of dark matter halos, there are two steps required to simulate luminous galaxies with ellipticities. Firstly we need to populate the halos with galaxies, for which, in this paper, we use the conditional luminosity function (CLF) of Cooray & Milosavljević (2005), and secondly we need to assign ellipticities. We follow HRH and H04 in relating the ellipticities e of the galaxies to the ellipticity of the halo (the ‘elliptical’ model) or via the angular momentum of the halo (the ‘spiral’ model). In this section we first describe the CLF halo occupation model, and then discuss the elliptical, spiral and galaxy mix models that we use in the analysis that follows.

The CLF, denoted by $\Phi(L|M_h, z)$ gives the average number of galaxies with luminosities between L and $L + dL$ that reside in halos of mass M_h at a redshift of z . The CLF model is separated into terms associated with central and satellite galaxies with a further division into early-type and late-type galaxies. The free model parameters are then constrained in Cooray (2006) by observations of the galaxy luminosity function and galaxy correlation function over a wide range of redshift samples (for example the SDSS at $z < 0.1$ (Zehavi et al. 2004) and the COMBO-17 survey at $0.4 < z < 0.8$ (Wolf et al. 2003)). The results of this analysis show a very convincing match between CLF model predictions and observational results at all redshifts and thus provide an adequate model with which to populate simulated dark matter halos with luminous galaxies. The average number of galaxies that reside in a halo of mass M_h at redshift z is given by $N(M_h, z) = \int dL \Phi(L|M_h, z)$ where the luminosity ranges from the faintest observable magnitude (which we set to a typical ground-based survey depth of $r < 25.5$), to an absolute brightest galaxy magnitude $M_r > -23$. We use the best fit Cooray (2006) CLF parameters or the chosen fiducial values in the cases where the parameters are poorly constrained. This results in a realistic redshift distribution of the foreground galaxies with roughly 15 galaxies per square arcmin with $z < 1.0$.

We use three simple galaxy models which we term, ellipticals, spirals and mix. Ellipticals are defined to have the same ellipticity as their parent halos. Spirals are modelled as a thick disk randomly misaligned with the angular momentum vector of its parent halo, with a mean misalignment angle of 20° as suggested by the results of van den Bosch et al. (2002) and discussed in more detail

in H04. Note that for completeness, we also present the results, in section 3, for a spiral model where the disk is aligned with the angular momentum vector of its parent halo, as in HRH. The results in the shear-ellipticity correlation analysis that follow in section 4, however, are unaffected by whether the disk is misaligned or not, and we therefore only present the shear-ellipticity correlation results from our misaligned spiral model. Our mix model populates dark matter halos with the same elliptical or misaligned spiral galaxies according to the early-type and late-type CLFs of Cooray (2006). These CLFs are constrained such that they reproduce the luminosity functions and clustering properties of red and blue galaxies. Our simple galaxy ellipticity models will clearly break down in the case of parent halos which host more than one galaxy. We therefore limit our study to singly occupied halos which satellite galaxies are unlikely to inhabit. For our mix model, this criterion results with roughly one third of the halos populated with elliptical galaxies at all redshifts.

In this paper we determine the ellipticity parameters ε_i for each galaxy, where ε_i for a perfect ellipse with axial ratio β at position angle θ , is given by,

$$\begin{pmatrix} \varepsilon_1 \\ \varepsilon_2 \end{pmatrix} = \frac{1 - \beta^2}{1 + \beta^2} \begin{pmatrix} \cos 2\theta \\ \sin 2\theta \end{pmatrix}. \quad (3)$$

In order to study the effect of these intrinsic galaxy shapes on weak lensing measurements we then define and use the alternative ellipticity parameters e_i given by

$$e_i = \frac{\varepsilon_i}{2R}, \quad (4)$$

where the responsivity R is a correction to account for the response of an ensemble of galaxies to weak lensing shear (Rhodes et al. 2000; Bernstein & Jarvis 2002). Without this responsivity correction to our ellipticity measurements, equation 1 would not apply. For the following unweighted analysis, $R = 1 - \langle \varepsilon_i^2 \rangle = 0.89$ for all galaxy models (although note that for simplicity in HRH and H04 the responsivity R was set equal to 1). The resulting e_i ellipticity distributions have a mean $\langle e_i \rangle = 0$ and a width $\sigma_e = 0.33$ which is very similar to what is measured from space-based data (Heymans et al. 2006).

3 INTRINSIC GALAXY ALIGNMENTS

In this section we update the analysis of HRH and H04 by re-measuring the intrinsic alignment correlation $\langle e_s^a e_s^b \rangle$ from simulations. The N-body simulation used in this analysis is at a significantly higher resolution than the VIRGO simulations (Jenkins et al. 1998) used by HRH allowing for more reliable measurements of halo angular momentum. It also covers a larger cosmological volume and thus yields higher signal-to-noise measurements. The evolution of the large-scale structure is now preserved, permitting a direct measurement of the E and B modes of the angular intrinsic alignment correlation. As a result we do not have to rely on projecting a measured real space correlation function into an angular correlation function using weakly constrained redshift dependent galaxy clustering models. The analyses of the simulations differ slightly in the fact that we now populate halos according to the CLF of Cooray (2006) instead of introducing low and high mass cuts to remove halos less likely to harbour a single galaxy. Our galaxy models are however identical, with the new addition of the mix model. The intrinsic ellipticity correlation $\eta(r_{ab})$, is given by

$$\eta(r_{ab}) = \langle e_t(\mathbf{r}_a) e_t(\mathbf{r}_b) \rangle + \langle e_r(\mathbf{r}_a) e_r(\mathbf{r}_b) \rangle, \quad (5)$$

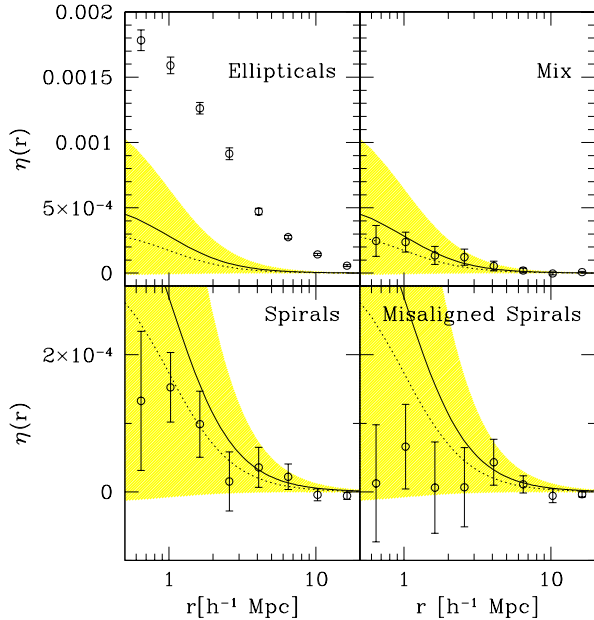


Figure 1. The intrinsic galaxy ellipticity correlation $\eta(r_{ab})$ as a function of comoving galaxy separation r_{ab} as measured from the simulation assuming three different galaxy models; ellipticals, spirals (placed perpendicular to the angular momentum vector as in HRH, lower left, and misaligned, as in H04 and the rest of this paper, lower right) and mix. The shaded region shows the 95% confidence region constrained from measurements of intrinsic galaxy alignments in the SDSS Mandelbaum et al. (2006), where the best-fit is over-plotted (solid). The best fit model from the misaligned spiral galaxies measured in H04 is shown dotted.

where the comoving galaxy separation $r_{ab} = |\mathbf{r}_a - \mathbf{r}_b|$, and $\langle e_t e_t \rangle$ and $\langle e_r e_r \rangle$ are the tangential and rotated correlation functions (see for example H04). The measured $\eta(r_{ab})$ is shown in Figure 1 for each galaxy model, where for completeness we have also included the HRH spiral model where the disk is placed perpendicular to the angular momentum vector of the halo. The shaded region in each plot is the 1σ confidence region for $\eta(r_{ab})$ as constrained from measurements of intrinsic galaxy alignments in the SDSS (Mandelbaum et al. 2006). The strength of the signal for the elliptical model at separations $r > 3h^{-1}\text{Mpc}$ is inconsistent with the SDSS results at the 6σ level and we can thus reject this model at 99.9% confidence. The spiral and mix models are consistent with the SDSS constraints. All results are consistent with the previous results from HRH and H04, and now supersede those constraints.

Following H04, we provide parameter fits to these results using the following model

$$\langle e_i(\mathbf{r}_a) e_i(\mathbf{r}_b) \rangle = \frac{A}{1 + (r_{ab}/B)^2}, \quad (6)$$

where the amplitude A is chosen to be a free parameter. For the elliptical model, B is also allowed to be a free parameter. For all other models B constrained to $B = 1h^{-1}\text{Mpc}$. Table 1 compares the best fitting parameters for the tangential $\langle e_t e_t \rangle$ and rotated $\langle e_r e_r \rangle$ and rotated $\langle e_r e_r \rangle$ ellipticity correlation functions, as well as the total ellipticity correlation $\eta(r_{ab})$. For the elliptical model, both A and B are free parameters. For all other models B is constrained to be $B = 1h^{-1}\text{Mpc}$. The best fits to the results presented in this paper can be compared to the result from H04 (referred to as HRH* in that paper) and Mandelbaum et al. (2006) (SDSS), where

Model	Parameter	$\langle e_t e_t \rangle$	$\langle e_r e_r \rangle$	$\eta(r_{ab})$
Ellipticals	$A/10^{-3}$	$1.47^{+0.05}_{-0.02}$	$0.38^{+0.18}_{-0.08}$	$1.75^{+0.08}_{-0.02}$
	B	$2.94^{+0.07}_{-0.04}$	$0.96^{+0.40}_{-0.30}$	$2.77^{+0.09}_{-0.07}$
Mix	$A/10^{-3}$	$0.45^{+0.10}_{-0.05}$	$0.07^{+0.08}_{-0.05}$	$0.47^{+0.13}_{-0.07}$
Spirals	$A/10^{-3}$	$0.30^{+0.05}_{-0.02}$	$-0.02^{+0.07}_{-0.05}$	$0.28^{+0.10}_{-0.05}$
Misaligned	$A/10^{-3}$	$0.15^{+0.08}_{-0.02}$	$0.00^{+0.05}_{-0.02}$	$0.07^{+0.10}_{-0.05}$
HRH*	$A/10^{-3}$	-	-	0.35 ± 0.16
SDSS	$A/10^{-3}$	-	-	0.57 ± 0.72

Table 1. The intrinsic alignment amplitude A and scale length B as defined in equation 6 for the tangential $\langle e_t e_t \rangle$, and rotated $\langle e_r e_r \rangle$ ellipticity correlation functions, as well as the total ellipticity correlation $\eta(r_{ab})$. For the elliptical model, both A and B are free parameters. For all other models B is constrained to be $B = 1h^{-1}\text{Mpc}$. The best fits to the results presented in this paper can be compared to the result from H04 (HRH*) and Mandelbaum et al. (2006) (SDSS), where we have included a scaling factor of $4R^2$ to account for the shear responsivity (equation 4) that we include in this analysis. The quoted errors are all 1σ , except in the case of SDSS which corresponds to a 3σ constraint.

we have included a scaling factor of $4R^2$ to account for the shear responsivity (equation 4) that we include in this analysis. It is interesting to note that the rotated component of the ellipticity correlation function $\langle e_r e_r \rangle$, is found to be weaker than the tangential component $\langle e_t e_t \rangle$, which is in contrast to previous assumptions that $\langle e_t e_t \rangle \simeq \langle e_r e_r \rangle$.

Taking all halos between a redshift of $0 < z < 1$ we measure the angular galaxy ellipticity correlation $\langle e_s(\theta_a) e_s(\theta_b) \rangle$, directly from the simulations. Crittenden et al. (2002) show that the correlation functions can be decomposed into the following E- and B-type correlators,

$$\xi^E(\theta) = \frac{\xi_+(\theta) + \xi'_-(\theta)}{2} \quad \xi^B(\theta) = \frac{\xi_+(\theta) - \xi'_-(\theta)}{2} \quad (7)$$

where, in this case,

$$\xi_{\pm}(\theta) = \langle e_t e_t \rangle_{\theta} \pm \langle e_r e_r \rangle_{\theta}, \quad (8)$$

and

$$\xi'_-(\theta) = \xi_-(\theta) + 4 \int_{\theta}^{\infty} \frac{d\vartheta}{\vartheta} \xi_-(\vartheta) - 12\theta^2 \int_{\theta}^{\infty} \frac{d\vartheta}{\vartheta^3} \xi_-(\vartheta). \quad (9)$$

Following the method detailed in Pen et al. (2002), we have decomposed the ellipticity correlation functions into their E and B modes $\xi^{E/B}$, assuming that $\langle e^a e^b \rangle_{\theta} = 0$ for $\theta > 20$ arcmin. Note that we treat each realization of the N-body simulations as an independent pointing and plot the mean and co-variance between the results from each realisation. The results are shown in Figure 2 where the measured E-mode can be compared to the expected ΛCDM shear correlation from a weak lensing survey with median redshift $z_m \sim 0.7$. This redshift corresponds to the median redshift of the galaxies, or the populated halos, in the simulations. For both the spiral and mix models, the signal is consistent with zero on all scales, although see H04 for a noise-free E/B mode analysis of the expected angular correlation signal from the best-fitting model to $\eta(r_{ab})$, which is directly applicable to the spiral and mix models analysed in this work. The elliptical model exhibits strong E and B modes out to $\theta < 10$ arcmin, although the small angle B-mode are consistent with zero. Figure 3 shows the E/B mode decomposition of the elliptical model signal when we have repeated

the analysis removing galaxy pairs that have a physical separation of $r_{ab} < 10h^{-1}\text{Mpc}$, the resulting E and B mode signal is consistent with zero on all scales, as expected.

3.1 Intrinsic Galaxy Alignment with Voids

We follow the analysis of Trujillo et al. (2006) to determine the degree of alignment between the rotation axis of galaxies located on the shells of cosmic voids, and the surface of those voids. We use a section of the simulation at fixed output time $z \sim 0.325$ and take all halos with mass $M_h > 8.5 \times 10^{11} h^{-1} M_\odot$ yielding a similar number density of the 2dFGRS and SDSS surveys analysed by Trujillo et al. (2006). Voids are selected using the same method of Patiri et al. (2006) and for each galaxy within $r_{\text{void}} < r < r_{\text{void}} + 4h^{-1}\text{Mpc}$ of the void centre (which has radius r_{void}) we calculate $\cos(\theta) = \mathbf{r} \cdot \mathbf{L} / (|\mathbf{r}| |\mathbf{L}|)$ where \mathbf{L} is the angular momentum of the parent halo. Figure 4 shows the resulting distribution of galaxies residing on the surface of voids with $0 \leq \theta \leq 90$ degrees. The errors come from a bootstrap analysis, and the solid line is the average result when the halo angular momenta are randomised. We find a distribution that is consistent with the null hypothesis that the angular momentum vector of halos near voids is randomly oriented with respect to the centre of voids. For our spiral galaxy model, where galaxy orientation is determined by the angular momenta of the parent dark matter halo, this result implies that no significant correlation exists between the orientation of galaxies and the centre of nearby voids in our simulations. This is in contrast to the Trujillo et al. (2006) detection results, which are over-plotted on figure 4 that can reject this null hypothesis at the 99.7% confidence level. These results are well fitted by the analytic prediction of Lee (2004), (shown dot-dashed). We discuss this difference further in section 6.

4 SHEAR-ELLIPTICITY CORRELATIONS

In this section we present shear-ellipticity correlation functions and their E/B mode decomposition for the three different galaxy models, as described in section 2.1. Figure 5 shows the measured correlation $\langle \gamma e \rangle$ between foreground galaxy ellipticity e (where the foreground galaxies have redshifts $0 < z < 1$) and the gravitational shear γ experienced by a set of background source galaxies at $z_s \sim 1$ where

$$\langle \gamma e \rangle_\theta = \langle \gamma_t(\theta_a) e_t(\theta_b) \rangle + \langle \gamma_r(\theta_a) e_r(\theta_b) \rangle. \quad (10)$$

Note that we treat each realization of the N-body simulations as an independent pointing and plot the mean and variance between the results from each realisation. This result represents the level of contamination that one would expect from each galaxy model for a deep lensing survey with a median redshift $z_m \sim 1$. These results show an anti-correlation, as predicted by Hirata & Seljak (2004) and measured by Mandelbaum et al. (2006). The strongest signal is found from the elliptical model, where all occupied halos contain a galaxy whose shape is the same as its parent dark matter halo. The spiral model shows a correlation that is consistent with zero on all scales, and the mix model shows a weak but significant anti-correlation on scales $\theta < 20$ arcmin. For reference, the solid theory curve shows the the shear-shear correlation function (multiplied by -1) for a deep $z_s = 1$ survey using the adopted ΛCDM cosmology. Note that the shear-ellipticity correlation for the mix model has a similar magnitude to the models tested in King (2005). In contrast however, we find signal that has power out to angular scales that

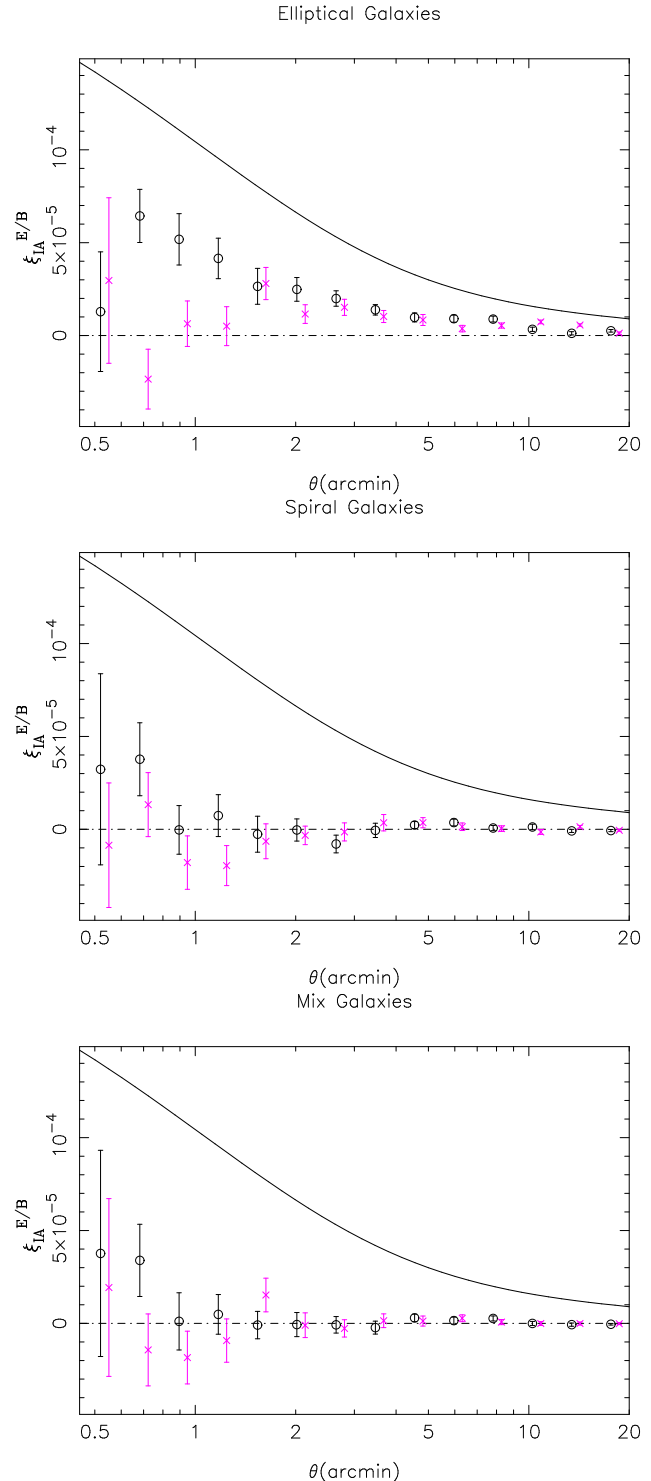


Figure 2. The E mode (circle) and B mode (cross) decomposition of the angular intrinsic galaxy ellipticity correlation $\langle e_s^a e_s^b \rangle_\theta$ as a function of angular galaxy separation on the sky, θ . This is measured from the simulation assuming three different galaxy models; ellipticals (upper panel), spirals (middle panel) and mix (lower panel). The resulting E-mode can be compared to the expected shear correlation (solid line) from a weak lensing survey with median redshift $z_m = 0.7$, which corresponds to the median redshift of the galaxies in the simulations. For clarity the B-mode points are slightly offset to the right.

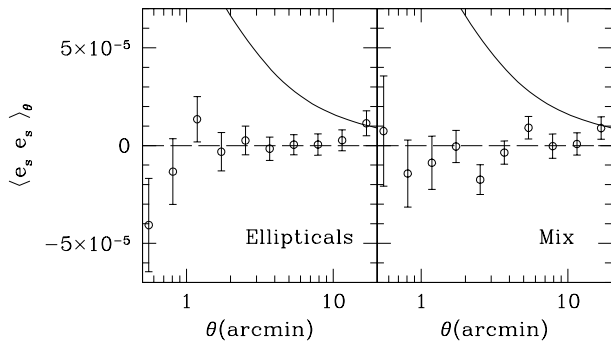


Figure 3. The measured angular intrinsic galaxy ellipticity correlation $\langle e_s^a e_s^b \rangle_\theta$ as a function of angular galaxy separation on the sky, θ when galaxy pairs that have a physical separation of $r_{ab} < 10h^{-1}\text{Mpc}$ are removed from the analysis. This is measured from the simulation assuming the elliptical galaxy model (right) and mix galaxy model (left). The shear correlation from a weak lensing survey with median redshift $z_m = 0.7$, which corresponds to the median redshift of the galaxies in the simulations, is shown for reference (solid line).

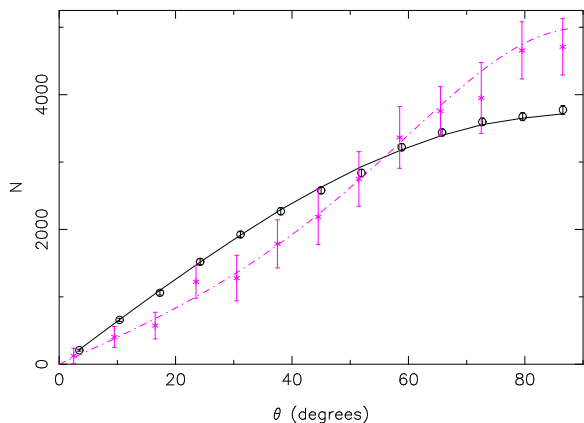


Figure 4. The distribution of galaxies residing near a void as a function of their degree of alignment between the rotation axis of the galaxies and the surface of the void (circles). For a perfectly aligned set of galaxies we would expect to see a peak at $\theta = 90^\circ$. Instead our result is consistent with the null hypothesis that galaxies are randomly oriented with all values of $\cos(\theta)$ equally likely. The errors come from a bootstrap analysis, and the solid line is the average result when the halo angular momenta are randomised. Our results can be compared with the observational results of Trujillo et al. (2006) (crosses) and the best fitting analytical prediction to these results from Lee (2004), shown dot-dashed.

are significantly larger than the 1 arcmin cut-off considered in King (2005).

Table 2 details the level of contamination to a weak lensing measurement by a shear-ellipticity correlation from each galaxy model, for both a deep $z_s \sim 1$ survey, whose results are plotted in figure 5, and medium deep $z_s \sim 0.5$ survey. The mix model shows a level of shear-ellipticity correlation which is $-6 \pm 1\%$ of the lensing signal at an angular scale $\theta = 1$ arcmin for the deep $z_s \sim 1$ survey.

Figure 6 shows the shear-ellipticity correlation function $\langle \gamma e \rangle$ for the mix galaxy model for two samples of galaxies split by mass. The strongest shear-ellipticity correlation is seen for the most massive galaxy sample where $M_h > 1.0 \times 10^{12} h^{-1} M_\odot$. This is expected, as the strength of the lensing shear is proportional

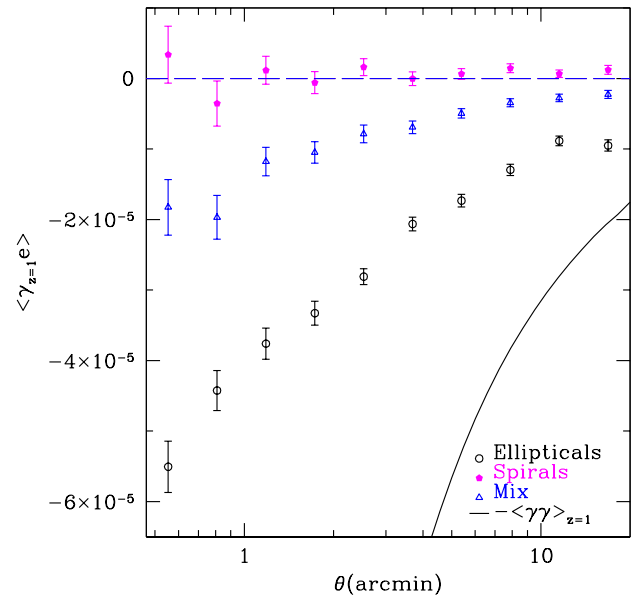


Figure 5. The shear-ellipticity correlation function $\langle \gamma e \rangle_\theta$ for the elliptical (circles), spiral (triangle) and mix (filled) galaxy models. In this result all source galaxies (that experience a lensing shear γ) are placed at a source redshift $z_s = 1$. The foreground galaxies, with intrinsic ellipticity e , populate the redshift space $0 < z < 1$. These results are tabulated in table 2 along with the results for a survey where all source galaxies are placed at $z_s = 0.5$. For reference, the solid theory curve shows the shear-shear correlation function (multiplied by -1) for a deep $z_s = 1$ survey using the adopted ΛCDM cosmology.

$z_m \sim 1$	$\theta \sim 0.5$	$\theta \sim 1$	$\theta \sim 10$
Elliptical	$-19 \pm 1\%$	$-20 \pm 1\%$	$-31 \pm 2\%$
Spirals	$1 \pm 1\%$	$1 \pm 1\%$	$2 \pm 2\%$
Mix	$-6 \pm 1\%$	$-6 \pm 1\%$	$-10 \pm 2\%$
$z_m \sim 0.5$	$\theta \sim 0.5$	$\theta \sim 1$	$\theta \sim 10$
Elliptical	$-67 \pm 5\%$	$-43 \pm 5\%$	$-82 \pm 8\%$
Spirals	$8 \pm 5\%$	$3 \pm 5\%$	$-10 \pm 8\%$
Mix	$-24 \pm 4\%$	$-14 \pm 5\%$	$-31 \pm 8\%$

Table 2. The percentage of contamination to a measurement of the shear-shear correlation function by a shear-ellipticity correlation from each galaxy model at $\theta = 0.5, 1.0, 10.0$ arcmin. Results are given for both a deep $z_s \sim 1$ lensing survey (upper rows), whose results are plotted in figure 5, and medium deep lensing $z_s \sim 0.5$ survey (lower rows).

to the mass of the lens. It is also reminiscent of what is seen in Mandelbaum et al. (2006), where the strongest signal is measured from the most luminous and hence the most massive galaxy sample. This result allows us to briefly discuss the impact of multiply-occupied halos, which we have removed from our analysis as a result of our uncertainty in how to connect the properties of the parent dark matter halo to the luminous galaxy members. One could consider the case where the central galaxy is represented by our elliptical model and the satellite galaxies are randomly oriented. The multiply occupied halos are typically the more massive halos, and we would therefore expect to see a strong signal from the central galaxies, as seen with the most massive galaxy sample shown in fig-

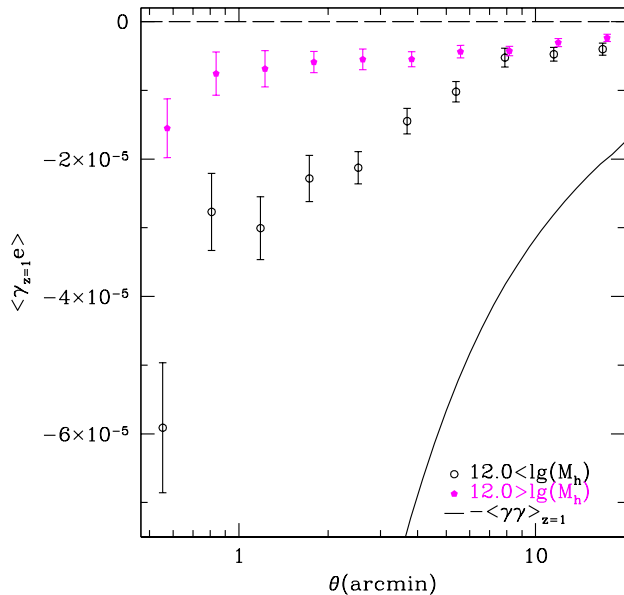


Figure 6. The shear-ellipticity correlation function $\langle \gamma e \rangle_{\theta}$ for the mix galaxy model for two samples of galaxies split by mass; where $M_h > 1.0 \times 10^{12} h^{-1} M_{\odot}$ (open) and where $M_h < 1.0 \times 10^{12} h^{-1} M_{\odot}$ (filled). Note that all source galaxies (that experience a lensing shear γ) are placed at a source redshift $z_s = 1$ and that for reference, the solid theory curve shows the the shear-shear correlation function (multiplied by -1) for a deep $z_s = 1$ survey using the adopted Λ CDM cosmology.

ure 6. Randomly oriented satellite galaxies would not contribute to the shear-ellipticity correlation signal and would thus dilute effect of the central galaxy. The reality of this scenario is however difficult to quantify, and indeed there is evidence that suggests satellite galaxies are not randomly oriented with a tendency to align with the major axis of the central galaxy (Brainerd 2005; Yang et al. 2006). We therefore limit our discussion, in the rest of this paper to singly-occupied halos, deferring a quantitative analysis that includes satellite galaxies for a future paper analysing higher resolution N-body simulations.

Following Crittenden et al. (2002) and the method detailed in Pen et al. (2002), we decompose the measured shear-ellipticity correlation functions into their E and B modes, equation 7, assuming that $\langle \gamma e \rangle_{\theta} = 0$ for $\theta > 20$ arcmin. Figure 7 shows the resulting E and B mode signals for all three galaxy models. As expected the E and B modes from the spiral model are consistent with zero. For the mix and elliptical models, the B-modes are negative but weaker than the corresponding E-modes. The B-modes are however fairly constant on scales $\theta < 15$ arcmin and would therefore be detectable if all B-modes from other non-lensing sources, such as residual point-spread function distortions, are negligible.

4.1 Redshift dependence

In this section we measure the dependence of the shear-ellipticity correlation signal as a function of the foreground galaxy redshift. We present the results for the elliptical model as the strength of the signal allows us effectively to probe the redshift dependence in the presence of increased noise from the redshift binning. The trends seen with the elliptical model are also seen with the mix model,

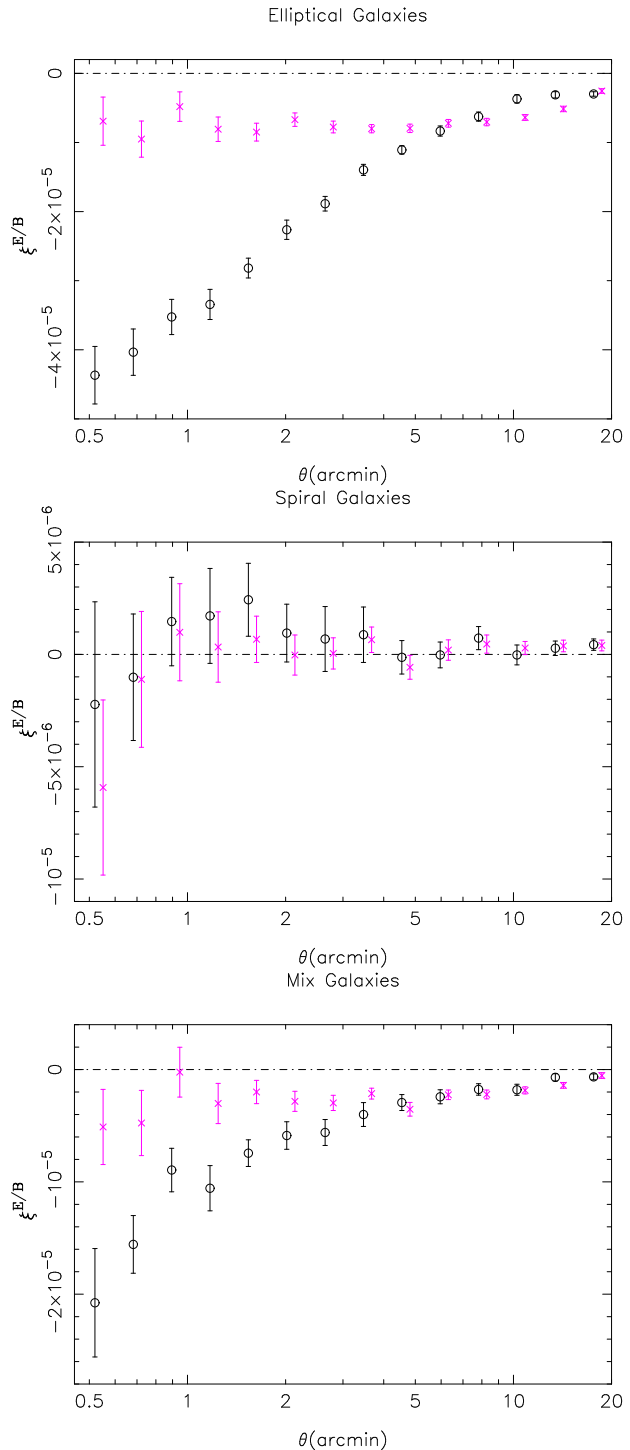


Figure 7. The E mode (circle) and B mode (cross) of the shear-ellipticity correlation function for the elliptical (upper panel), spiral (middle panel) and mix (lower panel) galaxy models. For clarity the B mode points are slightly offset to the right.

although at lower significance, and the shear-ellipticity correlation for the spiral model remains consistent with zero for all redshift slices.

Figure 8 shows the redshift dependent shear-ellipticity correlation for 5 different galaxy redshift slices; $0.0 - 0.4$, $0.4 - 0.65$, $0.65 - 0.75$, $0.75 - 0.85$, $0.85 - 0.95$. This result demonstrates

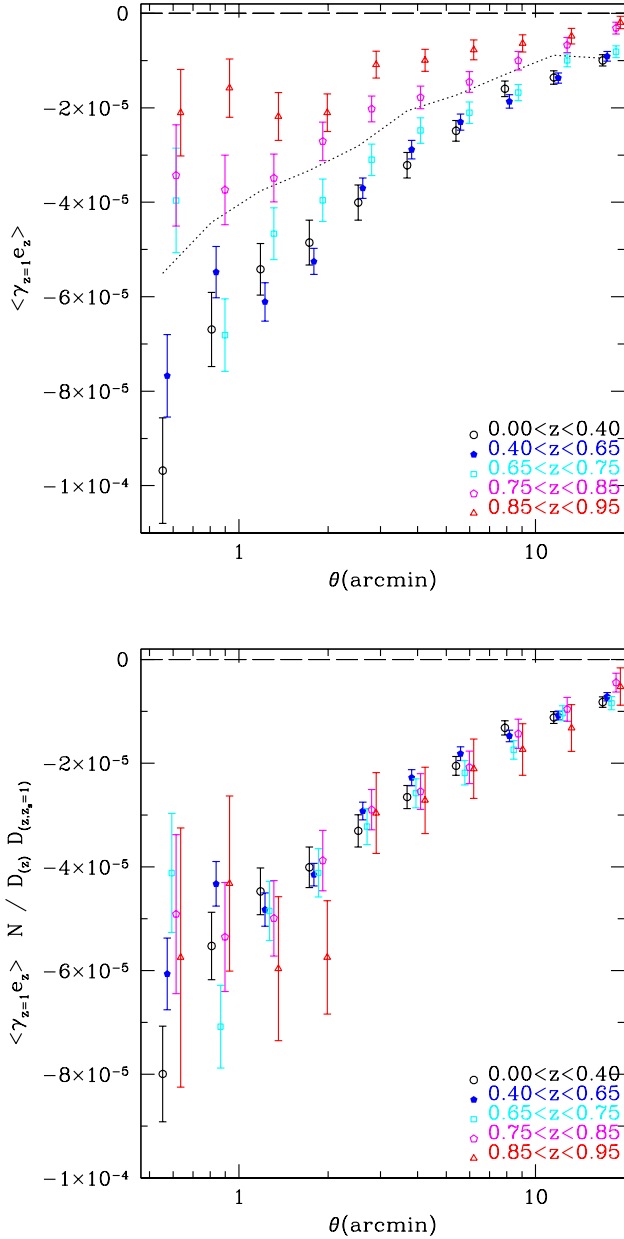


Figure 8. The redshift dependence of the shear-ellipticity correlation as a function of galaxy redshift slice z_l . The upper panel shows the measured signal for the following galaxy redshifts; $0.0 < z_l < 0.4$ (circle), $0.4 < z_l < 0.65$ (solid), $0.65 < z_l < 0.75$ (square), $0.75 < z_l < 0.85$ (hexagon), $0.85 < z_l < 0.95$ (triangle). The dashed line shows the elliptical measurement in Figure 5 from the full galaxy sample $0.0 < z_l < 1.0$. The lower panel shows the same signal with the lensing efficiency E factored out and normalized to the lensing efficiency N of the mean galaxy redshift of the full galaxy sample where $z_l = 0.68$

that the most significant anti-correlation is found for the low redshift ($z < 0.65$) galaxy samples, which are the most efficient for lensing source galaxies at $z_s = 1$. The lensing efficiency E of the lens-source pair is defined to be

$$E = \frac{D_l D_{ls}}{D_s} \quad (11)$$

Elliptical Galaxies

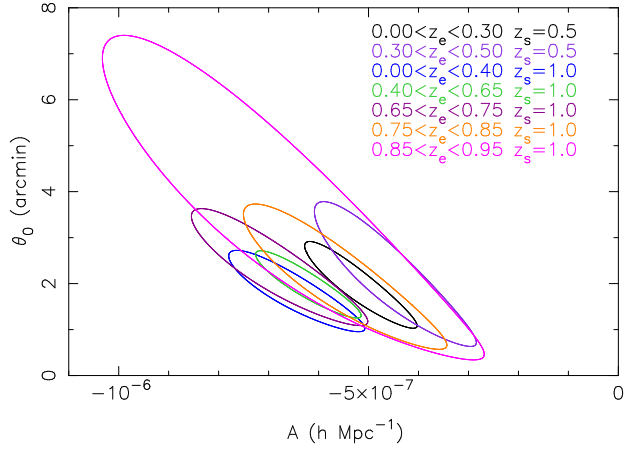


Figure 9. 2σ constraints on the amplitude A and scale dependence θ_0 (equation 12) of the shear-ellipticity correlation assuming the elliptical galaxy model. Parameter constraints are determined from the 5 different galaxy redshift slices shown in figure 8 where γ is measured at $z_s = 1.0$, plus 2 additional low redshift slices where γ is measured at $z_s = 0.5$.

where the distances D are all comoving angular diameter distances to the lens D_l , to the source D_s , and between the lens and source D_{ls} . We might expect the shear-ellipticity correlation signal to scale with the lensing efficiency and to test this hypothesis, the lower panel of figure 8 shows the shear-ellipticity correlation signal with the lensing efficiency factored out; we divide by E for the median lens redshift in each redshift slice, and multiply by a normalising factor N set equal to the lensing efficiency E of the mean redshift lens for the whole halo sample where $z_l = 0.68$. The result shows that the redshift dependent shear-ellipticity correlation measurements are very consistent with one another once the lensing efficiency is factored out. This then motivates the following parameterisation of the redshift evolution of the shear-ellipticity correlation,

$$\langle \gamma(z_s) e(z_l) \rangle_\theta = E \frac{A}{\theta + \theta_0}, \quad (12)$$

where the amplitude A and scale dependence θ_0 are free parameters. E is the lensing efficiency of the lens-source (γe) pair (equation 11), and z_l is set equal to the median redshift of each galaxy redshift slice. Note that this parameterisation is similar to the exponential parameterisation proposed by King (2005), but this functional form is found to produce a better fit to the results. Figure 9 shows the two parameter 2σ constraints on the amplitude A and scale dependence θ_0 as measured independently from the 5 different galaxy redshift slices shown in figure 8 where γ is measured at $z_s = 1.0$, plus 2 additional low redshift slices where γ is measured at $z_s = 0.5$. The consistent results for each galaxy redshift slice suggest that the evolution of the shear-ellipticity correlation can be safely modelled through the lensing efficiency of the lens-source pair.

Using this parameterisation (equation 12) we place constraints on the amplitude A and scale dependence θ_0 of the shear-ellipticity correlation measured jointly from the redshift dependent results. Figure 10 shows the resulting two-parameter 1 and 2σ constraints for the elliptical model (upper) and mix model (lower). The best fitting results for the elliptical model are $A = (-5.60 \pm 0.18) \times 10^{-7} h \text{ Mpc}^{-1}$ and $\theta_0 = 1.83 \pm 0.13$ arcmin. For the mix model

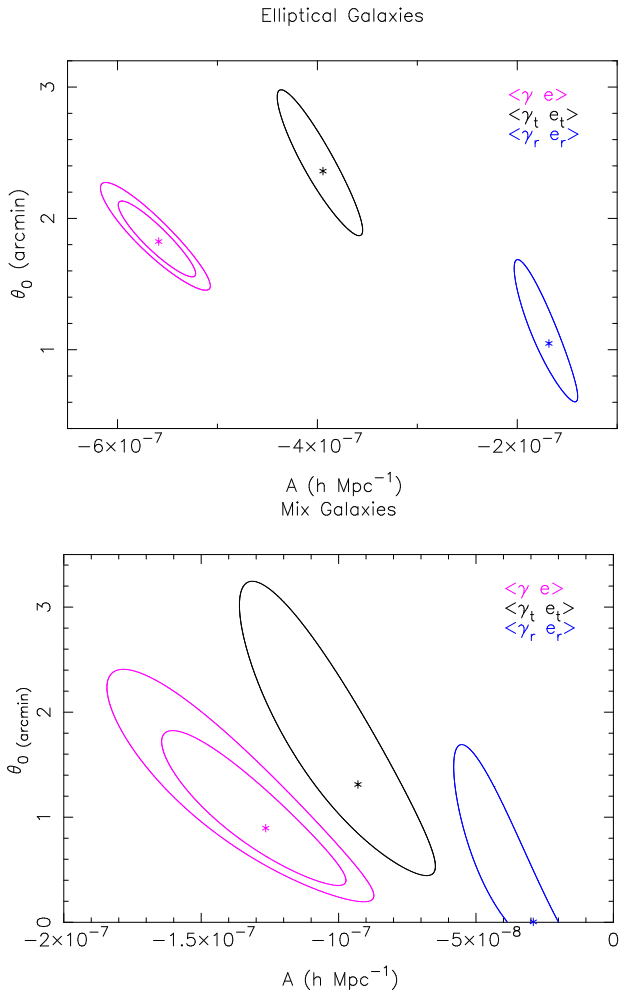


Figure 10. 1 and 2σ constraints on the amplitude A and scale dependence θ_0 (equation 12) of the shear-ellipticity correlation $\langle \gamma e \rangle$, assuming the elliptical galaxy model (upper) and mix galaxy model (lower). For clarity, only the 1σ constraints are shown for the tangential $\langle \gamma_t e_t \rangle$ and rotated $\langle \gamma_r e_r \rangle$ shear-ellipticity correlations, where $\langle \gamma_r e_r \rangle$ is the weakest signal. The best-fit parameters are marked with a star.

$A = (-1.29 \pm 0.16) \times 10^{-7} h \text{ Mpc}^{-1}$ and $\theta_0 = 0.93^{+0.38}_{-0.29}$ arcmin. The 1σ errors on A are marginalised over θ_0 and vice versa. The constraints measured for the tangential $\langle \gamma_t e_t \rangle$ and rotated $\langle \gamma_r e_r \rangle$ shear-ellipticity correlations are also shown in figure 10, but for clarity only the 1σ constraints are presented. Note that the $\langle \gamma_r e_r \rangle$ shear-ellipticity correlation is always weaker than the $\langle \gamma_t e_t \rangle$ shear-ellipticity correlation.

5 DISCUSSION

The results that have been presented in this paper and others (e.g. H04, Hirata & Seljak (2004); Mandelbaum et al. (2006)), demonstrate that if a relation exists between the shape of galaxies and the properties of their parent dark matter halos then there is the potential for contamination to the measurement of weak gravitational lensing by large-scale structure. The conclusion that one should draw from these works is that it is no longer acceptable to assume that all the intrinsic contributions to the observed galaxy ellipticity correlation function (i.e. terms that include e_s in equation 2)

are negligible. We must therefore seek to derive and apply optimal methods to remove these sources of contamination in the analyses of the next generation of weak lensing surveys. In this paper we have sought to answer the question, what level of contamination might one expect, and our conclusions are clearly dependent on our choice of galaxy model; ellipticals, spirals or mix.

A wealth of observational evidence allows us immediately to rule out the elliptical model on several grounds. The measurement of the intrinsic alignment signal $\eta(r)$ from the SDSS (Mandelbaum et al. 2006) is inconsistent with the elliptical model signal at the 99.9% level, as shown in Figure 1. Similar constraints could also be placed from the intrinsic alignment signal measured in the SuperCOSMOS survey (Brown et al. 2003). Figure 2 shows the expected angular ellipticity correlation in the absence of weak lensing for a survey with median redshift $z_m = 0.7$. This medium depth survey is similar to the Red sequence Cluster Survey (RCS) Hoekstra et al. (2002) and the CTIO survey (Jarvis et al. 2003). Weak lensing analyses of these two surveys constrain the amplitude of the matter power spectrum to be $\sigma_8 \sim 0.8 \pm 0.15$ for $\Omega_m = 0.3$, which is consistent with the results from the analysis of the cosmic microwave background (Spergel et al. 2006). If more than half of the RCS and CTIO measured lensing signal came from intrinsic alignments, as suggested by the results of the elliptical model, the ‘true’ value of σ_8 would be then be very low and inconsistent with other observational constraints. The COMBO-17 survey has been analysed using redshift weighting to remove the intrinsic contribution from close galaxy pairs (H04) and only a small difference was noted in the resulting signal, placing constraints on the intrinsic alignment contamination that would also reject the elliptical model at the 99% confidence level. Lastly, if the shear-ellipticity correlations were as strongly anti-correlated as expected from an elliptical model for median-deep surveys (see Table 2) we would expect to measure no weak lensing signal in the RCS and CTIO surveys, which is not the case. All of the evidence therefore suggests that not every galaxy has the same shape as its parent halo, and we can therefore rule out the 100% elliptical model.

The results from the spiral model are consistent with the Mandelbaum et al. (2006) SDSS constraints on intrinsic galaxy alignment. It predicts a very low intrinsic alignment correlation and low shear-ellipticity correlation that is consistent with zero on all scales. It is important however to take note of the SDSS results for their ‘L6’ massive elliptical galaxy sample (Mandelbaum et al. 2006). This sample of massive ellipticals exhibit a strong correlation between their galaxy shape and the surrounding density field. This observation has been propagated to high redshift to predict a measured shear-ellipticity anti-correlation that is $\sim 100\% \pm 50\%$ of the magnitude of the expected shear-shear correlation signal for a survey with $z_m = 1$. The amplitude of the ‘L6’ shear-ellipticity correlation is similar to the measured shear-ellipticity correlation signal from our elliptical model, but is inconsistent at the 4σ level with the measured shear-ellipticity correlation signal from our spiral model. In order to reproduce the strong SDSS signal from a subsample of galaxies in our simulations we therefore require a small population of elliptical galaxies and can thus rule out the 100% spiral model.

We have modelled a mixed population of spiral and elliptical galaxies using the early-type/late-type halo occupation distribution of Cooray (2006) which reproduces the observed luminosity functions and clustering properties of red and blue galaxies. The results from this mix model are consistent with all the observational results of Mandelbaum et al. (2006) It predicts low intrinsic alignment correlation, weak, though significant, shear-ellipticity corre-

lations, and negative B-modes. B-modes from systematics associated with the observations (for example residual distortions from the optical point-spread function) would typically produce positive B-modes and hence one would not expect to be able to detect the weakly negative B-mode signature of the mix model in current data.

The effect of the shear-ellipticity correlation is to reduce the measured shear-shear correlation below the amplitude of the true cosmological lensing signal. If uncorrected for, this would result in an underestimate of σ_8 from weak lensing measurements. The degree of underestimation would be survey depth dependent as from Table 2 we expect a medium-depth survey to suffer $\sim 20\%$ contamination and a deep survey to suffer $\sim 10\%$ contamination. A comparison of the results from different depth surveys should therefore, in principle, be able to constrain models of shear-ellipticity correlations as one would expect to measure lower values of σ_8 from shallower surveys. Whilst it is tempting to discuss the trend in the literature of somewhat higher σ_8 measurements from deeper lensing surveys, the uncertainties in the source redshift distribution (Van Waerbeke et al. 2006), sampling variance and shear calibration errors (Heymans et al. 2006) means that we are unable to make any firm conclusions with current lensing data to confirm or rule out the mix galaxy model.

5.1 Diagnostics for shear-ellipticity contamination

For the next generation of lensing surveys, the technical systematics associated with the detection and measurement of weak lensing have a promising chance of being negligible. A significant detection of negative B-modes would then suggest contamination from shear-ellipticity correlations. In addition, the results of Mandelbaum et al. (2006) and the comparison of the different models used in this analysis demonstrate that shear-ellipticity correlation is likely to be galaxy morphology dependent. For future multi-colour surveys with photometric redshifts one will be able effectively to separate red-sequence elliptical galaxies from the galaxy sample using a simple colour cut (see for example Bell et al. (2004)). With large area surveys one could then analyse the data with and without the elliptical galaxy population. A difference between the two measurements would suggest contamination from shear-ellipticity correlations. If that is the case, a zero B-mode measurement from an analysis where all elliptical-type galaxies have been rejected might well serve as a good indication that the contamination has been removed.

In section 4.1 we investigated the redshift dependence of the shear-ellipticity correlation $\langle \gamma_\alpha e_\beta \rangle$ where $z_\alpha < z_\beta$. The results, shown in figure 8 demonstrated that the evolution of the signal is proportional to the lensing efficiency E (equation 11) of the lens-source pair, where, for the shear-ellipticity correlation $\langle \gamma_\alpha e_\beta \rangle$ the source is at z_α and the lens is at z_β . The model that provides the most realistic description appears to be the mix model for which we have constrained the amplitude of the $\langle \gamma e \rangle$ signal to $\sim 10\%$ accuracy. We have calculated the level of contamination arising from a mixed galaxy population for a deep $z_m \sim 1$ survey analysed using the shear correlation function $\langle \gamma \gamma \rangle$, and found it to be at the level of $-6 \pm 1\%$ and $-10 \pm 2\%$ at angular scales 1 and 10 arcmin respectively. Using the $\langle \gamma e \rangle$ model (equation 12) with the best fitting parameters to our results, one could now potentially remove this contaminating signal to an accuracy of better than 1% of the lensing signal. We would urge caution with applying such a method however, as our results in section 3.1 clearly indicate the limitations of the simple models that we have used to link the properties of galaxies with their parent dark matter halos. We would there-

fore recommend using the $\langle \gamma e \rangle$ model (equation 12) that we have provided as a guide to the level of contamination, which should be self-consistently determined from the lensing data using the result that the contamination scales with lensing efficiency. As proposed by Hirata & Seljak (2004), measurements of cross-correlation tomography $\langle \gamma_\alpha \gamma_\beta \rangle$ (see for example Takada & White (2004)) will be a useful diagnostic tool, as the true cosmological lensing signal scales differently with redshift with the lensing efficiency integrated over all foreground lenses. One would therefore be able to project out the different redshift dependences of the two signals as demonstrated by King (2005) and simultaneously constrain the cosmological lensing signal and the contaminating shear ellipticity correlations.

6 CONCLUSION

We have investigated potential sources of contamination to the measurement of weak lensing by large-scale structure from the intrinsic alignment of galaxies, in section 3, and from the presence of shear-ellipticity correlations between foreground galaxy shapes and the weak lensing shear experienced by background galaxies, in section 4. These two sources of physical contamination behave rather differently. The intrinsic alignment contamination arises from close galaxy pairs, and can thus be eliminated by downweighting those galaxy pairs which are at close separations (Heymans & Heavens 2003; King & Schneider 2002), or by measuring cross-correlation tomography between different redshift bins. Intrinsic ellipticity-ellipticity correlations are thus not a problem if photometric redshifts are available. In contrast, the shear-ellipticity correlation arises from galaxy pairs which are at large physical separations, with the strongest correlations arising for lens-source pairs where the lensing efficiency E (equation 11) is at its strongest. This could potentially be directly eliminated through morphological galaxy selection, or from measuring weak lensing shear correlation within thin redshift slices (King 2005). All possible techniques to remove these sources of contamination will require good photometric redshift measurements and acquiring deep multi-colour data should be made a top priority for all future lensing surveys.

As discussed in section 5 the conclusions are dependent on the choice of model that we use to connect galaxy shape to the properties of its parent dark matter halo. General trends are that for deeper surveys, where the cosmological lensing signal is at its strongest, the degree of contamination is decreased. Eliminating the elliptical model through comparison to several observation results allows us to conclude that for medium deep surveys $z_m > 0.5$, intrinsic alignment contamination contributes only to the small angular scales $\theta < 1.5$ arcmin, and we refer the reader to H04 for a more detailed discussion on the implications of intrinsic galaxy alignments for future lensing surveys. The shear-ellipticity correlation is consistent with zero for our spiral model. To reproduce the results of Mandelbaum et al. (2006) however it is necessary to include a population of elliptical galaxies which introduce contamination to the shear lensing signal at the $\sim 10\%$ level for a deep $z_m = 1$ survey and $\sim 20\%$ level for a medium deep $z_m = 0.5$ survey (see table 2).

The galaxy models that we have applied to the simulations are indeed clear simplifications of reality as they consider only the properties of the parent halo, not the halo environment or the tidal density field directly. The non-detection of any alignment between a galaxy's spin axis and the surface of voids in our simulations, in section 3.1, is in some tension with the analysis of the 2dF and SDSS surveys (Trujillo et al. 2006). If the observation is robust, it

is therefore likely that it is not only the properties of the parent halo that impact on galaxy shape, but also the surrounding environment to some extent. In the rare cases of galaxies near voids or clusters, we might well expect the environment to have a stronger effect on galaxy shape than its parent dark matter halo and it will be important to investigate this further with full hydro-dynamical simulations on cosmological scales (see for example Navarro et al. 2004).

The important point to take away from this analysis is that our numerical study supports the notion that the contamination from shear-ellipticity correlation scales with lensing efficiency. This simple scaling with redshift offers possibilities of determining the cosmic shear signal and the contamination simultaneously, either by using the models constrained in section 4.1 for the behaviour of the contamination (cf King 2005), or by making fewer assumptions and parameterising the contamination. Because of the redshift scaling, only a single function needs to be parameterised. Cosmological parameter estimation would then proceed by marginalising over the nuisance parameters describing the contamination. Within the context of the model considered here, the $\langle\gamma e\rangle$ contamination can be estimated to an accuracy of 3% and 10% for the elliptical and mix models respectively.

A more detailed study of the redshift dependence of shear-ellipticity correlation will, however, be required for the more ambitious future lensing experiments which aim to determine $w(z)$. Such studies will need to include the satellite galaxy population that is missing from this analysis in addition to an improved mixed galaxy population model that takes into account an observationally constrained redshift evolution in the ratio of elliptical to spiral galaxies for different halo masses. This will require the development of better models for galaxy formation in dark matter simulations to improve our understanding of the connection between galaxies and their dark matter halos and the resulting impact on weak lensing studies. In the meanwhile we should rely on probing this phenomenon with existing data sets, in order to develop suitable diagnostics and analysis tools that will not subject weak lensing measurements to the kinds of contamination investigated in this paper thus allowing weak lensing to reach its full potential as a high precision dark matter and dark energy probe.

7 ACKNOWLEDGMENTS

We thank Rachel Mandelbaum and Chris Hirata for useful discussions on this project, Asantha Cooray for making code based on his CLF publicly available, and Ignacio Trujillo for providing us with his results and the analytical predictions of Lee (2004). We would also like to thank the referee for his/her helpful comments. The simulations used in this analysis were performed on the IBM-SP at NERSC. CH is supported by a CITA National fellowship and, along with LVW, acknowledges support from NSERC and CIAR. MW was supported in part by NASA and the NSF.

REFERENCES

- Bacon D., Massey R., Refregier A., Ellis R., 2003, MNRAS, 344, 673
 Bell E. F., Wolf C., Meisenheimer K., Rix H., Borch A., Dye S., Kleinheinrich M., Wisotzki L., McIntosh D. H., 2004, ApJ, 608, 752
 Bernstein G. M., Jarvis M., 2002, AJ, 123, 583
 Brainerd T. G., 2005, ApJL, 628, L101
 Brown M., Taylor A., Bacon D., Gray M., Dye S., Meisenheimer K., Wolf C., 2003, MNRAS, 341, 100
 Brown M., Taylor A., Hambly N., Dye S., 2002, MNRAS, 333, 501
 Catelan P., Kamionkowski M., Blandford R. D., 2001, MNRAS, 320, L7
 Cooray A., 2006, MNRAS, 365, 842
 Cooray A., Milosavljević M., 2005, ApJL, 627, L89
 Crittenden R., Natarajan R., Pen U., Theuns T., 2001, ApJ, 559, 552
 Crittenden R., Natarajan R., Pen U., Theuns T., 2002, ApJ, 568, 20
 Croft R. A. C., Metzler C. A., 2000, ApJ, 545, 561
 Davis M., Efstathiou G., Frenk C. S., White S. D. M., 1985, ApJ, 292, 371
 Hamana T., Miyazaki S., Shimasaku K., Furusawa H., Doi M., Hamabe M., Imi K., Kimura M., Komiyama Y., Nakata F., Okada N., Okamura S., Ouchi M., Sekiguchi M., Yagi M., Yasuda N., 2003, ApJ, 597, 98
 Heavens A., Peacock J., 1988, MNRAS, 232, 339
 Heavens A., Refregier A., Heymans C., 2000, MNRAS, 319, 649
 Heymans C., Bell E. F., Rix H.-W., Barden M., Borch A., Caldwell J. A. R., McIntosh D. H., Meisenheimer K., Peng C. Y., Wolf C., Beckwith S. V. W., Häußler B., Jahnke K., Jøgee S., Sanchez S. F., Somerville R. S., Wisotzki L., 2006, MNRAS Letters accepted
 Heymans C., Brown M., Heavens A., Meisenheimer K., Taylor A., Wolf C., 2004, MNRAS, 347, 895
 Heymans C., Brown M. L., Barden M., Caldwell J. A. R., Jahnke K., Rix H.-W., Taylor A. N., Beckwith S. V. W., Bell E. F., Borch A., Häußler B., Jøgee S., McIntosh D. H., Meisenheimer K., Peng C. Y., Sanchez S. F., Somerville R. S., Wisotzki L., Wolf C., 2005, MNRAS, 160
 Heymans C., Heavens A., 2003, MNRAS, 339, 711
 Heymans et al. C., 2006, MNRAS, 368, 1323
 Hirata C. M., Seljak U., 2004, Phys. Rev. D, 70
 Hoekstra H., Mellier Y., Waerbeke L. V., Fu E. S. L., Hudson M. J., Mao Li R., Parker L., Tereno I., Benabed K., 2006, A&A, accepted, astroph/0511089
 Hoekstra H., Yee H., Gladders M., 2002, ApJ, 577, 595
 Hoyle F., 1949, Problems of Cosmical Aerodynamics, p. 195
 Hu W., 1999, ApJ, 552, L21
 Jarvis M., Bernstein G., Jain B., Fischer P., Smith D., Tyson J., Wittman D., 2003, ApJ, 125, 1014
 Jenkins A., Frenk C., Thomas P., Colberg J., White S., Couchman H., Peacock J., Efstathiou G., Nelson A., 1998, ApJ, 499, 20
 Jing Y. P., 2002, MNRAS, 335, L89
 Kaiser N., Squires G., 1993, ApJ, 404, 441
 King L., Schneider P., 2002, A&A, 396, 411
 King L. J., 2005, A&A, 441, 47
 Lee J., 2004, ApJ, 614, L1
 Lee J., Pen U., 2001, ApJ, 555, 106
 Lee J., Pen U., Seljak U., 2002, ApJ, 543, L107
 Mackey J., White M., Kamionkowski M., 2002, MNRAS, 332, 788
 Mandelbaum R., Hirata C. M., Ishak M., Seljak U., Brinkmann J., 2006, MNRAS, 367, 611
 Massey R., Refregier A., Bacon D. J., Ellis R., Brown M. L., 2005, MNRAS, 359, 1277
 Navarro J. F., Abadi M. G., Steinmetz M., 2004, ApJL, 613, L41
 Patiri S. G., Betancort-Rijo J. E., Prada F., Klypin A., Gottlöber

- S., 2006, MNRAS, 369, 335
- Peebles J., 1969, ApJ, 155, 393
- Pen U.-L., Van Waerbeke L., Mellier Y., 2002, ApJ, 567, 31
- Porciani C., Dekel A., Hoffman Y., 2002, MNRAS, 332, 325
- Rhodes J., Refregier A., Collins N. R., Gardner J. P., Groth E. J., Hill R. S., 2004, ApJ, 605, 29
- Rhodes J., Refregier A., Groth E. J., 2000, ApJ, 536, 79
- Semboloni E., Mellier Y., Waerbeke L. V., Hoekstra H., Tereno I., Benabed K., Gwyn S., Fu L., Hudson M. J., Maoli R., Parker L., 2006, A&A, 452, 51
- Spergel et al. D., 2006, ApJ, submitted, astro-ph/0603449
- Takada M., White M., 2004, ApJL, 601, L1
- Trujillo I., Carretero C., Patiri S. G., 2006, ApJL, 640, L111
- Vale C., White M., 2003, ApJ, 592, 699
- van den Bosch F. C., Abel T., Croft R. A. C., Hernquist L., White S. D. M., 2002, ApJ, 576, 21
- Van Waerbeke L., Mellier Y., Hoekstra H., 2005, A&A, 429, 75
- Van Waerbeke L., Mellier Y., Radovich M., Bertin E., Dantel-Fort M., McCracken H., Fèvre O. L., Foucaud S., Cuillandre J., Erben T., Jain B., Schneider P., Bernardeau F., Fort B., 2001, A&A, 374, 757
- Van Waerbeke L., White M., Hoekstra H., Heymans C., 2006, Astroparticle Physics accepted astro-ph/0603696
- White M., 2002, ApJS, 143, 241
- Wolf C., Meisenheimer K., Rix H.-W., Borch A., Dye S., Kleinheinrich M., 2003, A&A, 401, 73
- Yang X., van den Bosch F. C., Mo H. J., Mao S., Kang X., Weinmann S. M., Guo Y., Jing Y. P., 2006, MNRAS, pp 528–+
- Zehavi et al. I., 2004, ApJ, 608, 16